THE JOURNAL OF PHYSICAL CHEMISTRY B

Article

pubs.acs.org/JPCB

Ligand Exchange Inducing Efficient Incorporation of CisPt Derivatives into Ureasil−PPO Hybrid and Their Interactions with the Multifunctional Hybrid Network

Eduardo F. Molina,*[,†,‡] Sandra H. Pulcinelli,[†] Celso V. Santilli,[†] and Valérie Briois*[,‡]

[†]Instituto de Química, UNESP, Rua Professor Francisco Degni, 55, 14800-900 Araraquara, SP, Brazil

[‡]Synchrotron SOLEIL L'Orme des Merisiers, BP48, Saint Aubin, 91192 Gif-sur Yvette, France

Supporting Information

ABSTRACT: Efficient incorporation of $(PtCl_3EtOH)^-$ anion derived from CisPt moiety into ureasil−PPO (poly(propylene oxide)) network was achieved from one-pot sol−gel synthesis carried out in the presence of water, HCl, and ethanol. Reactant proportion was adequately chosen to lead the sol−gel formation of siloxane nodes at the end of short PPO chains, to prevent the CisPt hydrolysis, and to induce platinum ligand exchange. The efficient dissolution of Pt species and the formation of a homogeneous liquid-like solution on the transparent and elastomeric ureasil−PPO hybrid were evidenced by differential scanning calorimetry and small-angle X-ray scattering. The CisPt ligand exchange and the formation of a Zeise-type salt $Y^+(PtCl_3R)^-$ were demonstrated by Raman spectroscopy and Pt L_3-edge EXAFS analysis. In light of these results and in agreement with the proportion of reactants introduced in the media for synthesis and those self-produced by hydrolysis and condensation processes, we proposed for R the ethanol moiety and for Y the ammonium cation. The Raman spectroscopy studies indicated also that the ammonium cations are coordinated by the ether-type oxygen atoms of the PPO chains backbone, whereas the amine groups of the urea linkage participate in the $(PtCl_3EtOH)^-$ anion coordination. *In situ* Raman monitoring of Pt species decomplexation induced by immersion of hybrid matrix in water highlighted the specific participation of Pt ligands in interaction with the urea group and of NH_4^+ cations coordinated by ether-type oxygen atoms in the formation of supramolecular interactions between the PPO chains. The electrospray mass spectrometry analysis of the Pt species released in water from the ureasil−PPO hybrid evidenced that the structure of the complex, NH_4 ($PtCl_3$ EtOH), incorporated in the matrix is totally preserved after delivery. Due to both well-known antitumoral and catalytic activities of Pt species, the results reported herein are of prime importance for further applications as drug delivery systems with optimized release pattern or as potential materials for new conceptual development of in situ catalyst delivery in homogeneous catalysis.

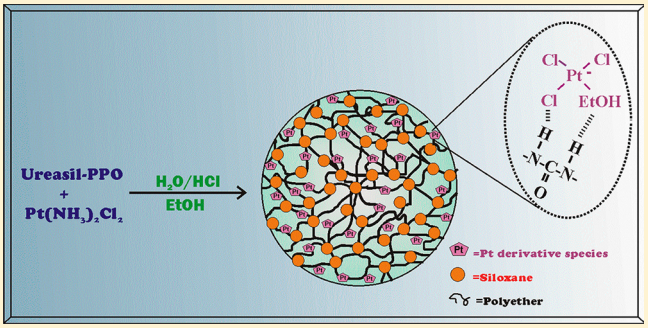

1. INTRODUCTION

During the two last decades, the design of new advanced organic−inorganic hybrid materials has been continuous in order to overcome the successive challenges imposed by the advent of new nanotechnologies[1−4] and satisfy the requirements for a variety of applications like physical, biological, and chemical sensors,[5−7] photochemical, electrochemical, and magnetic actuators,[8−10] controlled delivery,[11−14] selective separation,[15] and optical communication devices.[16−18] Many of these applications can be achieved using the versatile family of multifunctional materials based on the ureasil−polyether (PE) system which consists of PE chains of variable length grafted, at both ends, to siloxane domains by means of urea linkages (—NH(C═O)NH—).[19] This transparent elastomer and essentially amorphous material is thermally stable up to about 200 °C. Many interesting new PE based hybrid materials have already been prepared with properties tuned by the choice of guest molecules embedded in the hybrid host network. While the dissolution of alkali metal salts inside ureasil−PE provided good electrochemical properties,[19−21] the addition of lanthanide ions allowed the synthesis of multiwavelength emitters.[22−24] Recently the I_3^-/I^- redox couple was incorporated into the ureasil−PE electrolyte in order to produce robust quasi-solid-state dye sensitized solar cells.[25] Furthermore, controlled precipitation of iron oxide nanoparticles led to transparent magnetic materials with tunable interactions,[26,27] whereas an amperometric DNA biosensor for the detection and genotyping of the hepatitis C RNA virus in serum or plasma was recently developed from immobilization of streptavidin−biotinylated DNA probe into ureasil−polyethylene oxide (PEO) matrix.[28] Finally, the presence of both polar and nonpolar chemical groups with a tunable amount of hydro-

Received: March 19, 2012
Revised: June 5, 2012
Published: June 7, 2012

phobic domains was exploited in the development of a specific absorbent for removing organic pollutants from wastewater.[29]

Recently, the hydrogel-like feature achieved by the hydrophilic nature of polyethylene oxide (PEO), or the hydrophobic feature of polypropylene oxide (PPO), conjugated with the specific polarity of the urea linkage was used to promote the dissolution of different model drug molecules inside the ureasil−PE hybrid and then evaluate the efficiency of this material as a drug delivery device.[30,31] These works highlighted the possibility to fine-tune the sodium diclofenac (SDCF) delivery rate during short (days) and prolonged (weeks) periods by the judicious choice of PEO- and PPO-chain molecular weights (M_w), respectively. More recently, we took advantage of the release pattern observed for the swellable ureasil−PEO material to incorporate a high amount (5% w/w) of the antitumoral cisplatin molecule $[PtCl_2(NH_3)_2]$, CisPt, using a very simple one pot sol−gel route, and to achieve a multimodal release profile.[32] However, the one-pot sol−gel incorporation of CisPt on a less hydrophilic ureasil−PEO−PPO led to the precipitation of CisPt polycrystals and to the dissolution of Pt species inside the matrix chemically different from the CisPt molecules.[33] Actually, this new Pt species is only formed into ureasil−PPO hybrid matrix with M_w = 400 g mol^{-1}, which are labeled hereafter PPO400. These results evidence that the hybrid matrix is not a passive guest for the drug but can lead to its transformation toward new Pt species, named hereafter Pts. As the identification of this species is mandatory for further potential use in drug delivery systems, we studied in depth the formation of these Pts incorporated inside the PPO400 hybrid matrix.

Our aims in this paper are threefold. The first part is devoted to the identification of the new Pts incorporated inside the PPO400 hybrid matrix. Then we correlated in a second part the effects of the incorporation of Pts on the nanostructure and thermal behavior of the matrix. The ultimate goal of this study is the in-depth determination of interactions between the Pts and functional groups of the PPO400 network. This last part was mainly based on Raman spectroscopy analysis carried out for the as-prepared sample and also during the time-resolved *in situ* monitoring of the Pts-matrix decomplexation induced by its immersion in water.

2. EXPERIMENTAL SECTION

2.1. Sample Preparation. The ureasil cross-link agent was covalently bonded to both ends of the macromer by reacting the terminal aminopropyl groups of the end functionalized PPO (*O,O′-bis*(2-aminopropyl)-poly(propylene oxide) with 3-(isocyanatopropyl)-triethoxysilane) in a molar ratio of 1:2.[19] These commercially available reagents (Fluka, Aldrich) were stirred together into tetrahydrofuran (THF) under reflux for 15 h. Then, the THF solvent was eliminated by evaporation at 60 °C, hence forming the hybrid precursor $Si(EtO)_3(CH_2)_3NH$-(C═O)NHCHCH$_3$CH$_2$—(PEO)—CH$_2$CH$_3$CHNH(O═C)-NH$(CH_2)_3Si(OEt)_3$. This well-known synthesis procedure[21] was adopted for PPO with M_w = 400 g mol^{-1}. In a second step, silanol moieties (—Si$(OH)_3$) were generated, followed by condensation reactions to form ureasil cross-linking siloxane nodes. In order to avoid the hydrolysis of CisPt, an under-stoichiometric amount of water was used (H_2O/Si = 1.9) to hydrolyze the —Si$(OCH_2CH_3)_3$ groups under acid catalysis (HCl/Si = 0.13). Under these experimental conditions, the quantity of water produced by the condensation of Si−OH moieties is theoretically sufficient to complete the hydrolysis reaction of the precursor. A 37.5 mg portion of CisPt was incorporated into 1.5 g of the liquid hybrid precursor by adding 1.5 cm^3 of a water/ethanol mixture (0.015 vol/vol) containing 110 mg kg^{-1} of HCl catalyst.

2.2. Experimental Techniques. *DSC.* Differential scanning calorimetry measurements were carried out using a TA Instrument model Q100. Disk sections of approximately 20 mg were cut off from the hybrid matrix and placed in 0.04 cm^3 aluminum cans. Each sample was heated from −80 to 350 at 10 °C min^{-1}. The purge gas was high purity nitrogen supplied at 75 cm^3 min^{-1} flow rate.

SAXS. The nanostructure of materials was monitored by small-angle X-ray scattering measurements, performed at the SAXS beamline of the National Synchrotron Light Laboratory (LNLS, Campinas, Brazil). A vertical position-sensitive X-ray detector and a multichannel analyzer were used to record the SAXS intensity, $I(q)$, as a function of the modulus of the scattering vector $q = (4\pi/\lambda)\sin(\theta/2)$, with θ being the scattering angle and λ the radiation wavelength.

EXAFS. Pt L_3 edge XAS data were recorded on the SAMBA (Spectroscopies Applied to Materials Based on Absorption) beamline at SOLEIL (Saint Aubin, France).[34] A cylindrically bendable Pd coated mirror was used for collimating the beam at the entrance of the fixed exit sagitally focusing Si(111) double crystal monochromator. A second cylindrically bent Pd coated mirror was used to focus vertically the beam at the sample position. The grazing incidence of the white and monochromatic beams on both mirrors was set at 4 mrad, ensuring an efficient harmonic rejection. The EXAFS data of the as-prepared rubbery Pts-loaded PPO400 hybrid and of the CisPt, $K(PtCl_3NH_3)\cdot H_2O$, and $K(PtCl_3C_2H_4)\cdot H_2O$ crystalline references,[35−37] prepared as pellets, were recorded in transmission using ionization chambers filled with N_2/Ar gas mixture.

Analysis of the EXAFS data was performed using the Athena and Artemis graphical interface programs.[38] The data were Fourier-transformed between 4.7 and 13.7 Å^{-1} via a Kaiser−Bessel window with a *dk* of 2. To fit the EXAFS data, initial values of E_0 used for *k*-scaling and of S_0^2, the amplitude reduction factor, were obtained by fitting the EXAFS of the reference samples with numbers of nearest neighbor atoms (N) and distances (R) fixed at their expected crystallographic values.[35−37] The obtained values (E_0 = 11576 ± 2 eV, S_0^2 = 0.90 ± 0.10) were then used for the modeling of the EXAFS signals of the Pts-loaded hybrid. The fit quality is determined by the EXAFS reliability factor R_F which measures the relative misfit with respect to the data.

Raman. Raman data were recorded using the RXN1-785 Raman spectrometer from Kaiser Optical Systems, Inc. (KOSI), equipped with a NIR laser diode working at 785 nm as excitation light. A CCD detector provides a fast and simultaneous full spectral collection of Raman data from 100 to 3100 cm^{-1}. The laser beam was incident on the sample through a probe head equipped with optical fibers for the laser excitation and collection of the scattered Raman signals. The probe head was equipped with a short working distance objective lens (×10) for the measurement of Raman spectra of dried solid samples. A Mitutoyo long working distance objective lens (×20) was used for the time-resolved investigation of the Pts release from the hybrid matrix. The transmitted laser power at the sample position was 20 mW for dried samples and 70 mW for the release essay. 36 frames with an integration time of 50 s for each frame were merged for dried samples, whereas a total of 10 spectra with an integration

dx.doi.org/10.1021/jp302606b | J. Phys. Chem. B 2012, 116, 7931−7939

time of 6 s each were acquired during the release study. The release essay was carried out with the Pts-loaded hybrid immersed in deionized water heated at 37 °C under stirring. The water volume considered here was 20 times higher than that required for the solubilization of the nominal CisPt loaded in the hybrid. It is worth noting that the objective lens focuses the laser beam on the hooked hybrid sample immersed into water. Thus, the Raman measurements do only probe the Pts incorporated into the hybrid matrix, while the Pts species released in water solution are not detectable.

ESI-MS. The electrospray ion trap mass spectra (ESI-MS) of Pts released in water from the hybrid matrix were obtained with a LCQ Fleet analyzer (Thermo Scientific) using an acetonitrile/water mobile phase, a capillary vaporization nozzle at 275 °C, and ionization potential at 20 V. Water releasing solutions were injected directly into the spectrometer *via* a syringe pump with a flow rate of 0.02 cm^3 min^{-1}. Nitrogen gas was used for nebulization with flow rates of ≈20 cm^3 min^{-1}.

3. RESULTS AND DISCUSSION

3.1. Nature of CisPt Derived Species. During the one-pot sol−gel processing of CisPt-loaded PPO400 hybrid matrix, macroscopic transformations were observed. An opaque dark-yellow wet gel was first obtained after 1 h, suggesting the presence of CisPt species undissolved into the hybrid network. After drying under a vacuum at 70 °C for 72 h, a transparent light-yellow monolithic xerogel was obtained, indicating the formation of a homogeneous microstructure. The change of Raman bands located in the 300−400 cm^{-1} range recorded on the sample before and after drying clearly evidences the dissolution process of CisPt and the incorporation of a new CisPt derived species (see Figure S1 of the Supporting Information). The transparent light-yellow monolithic xerogel was then characterized in deep by EXAFS and Raman spectroscopies. It is noteworthy that the XRD pattern recorded for this xerogel did not present any diffraction peak preventing its use for identifying the newly formed Pts.

The Fourier transform of the EXAFS signals recorded for the hybrid sample is compared in Figure 1 to those recorded for crystalline reference compounds. These Fourier transforms present a main contribution between 1.0 and 2.5 Å assigned to the first coordination shell around Pt atoms. In the CisPt and $K(PtCl_3NH_3)\cdot H_2O$ crystalline references, the Pt atom is arranged in a 4-fold square planar coordination made of two nitrogen atoms at 2.05 Å and two chlorine atoms at 2.33 Å for the former[35] and one nitrogen atom at 2.04 Å and three chlorine atoms at an average distance of 2.30 Å for the second reference.[36] In the $K(PtCl_3C_2H_4)\cdot H_2O$ reference,[37] also known under the Zeise's salt name, the platinum atom is also square-planar, coordinated by three chlorine atoms at an average distance of 2.315 Å and two ethylenic carbon atoms at an average distance of 2.13 Å. Those structural parameters are satisfactorily obtained for the three investigated references, as reported in Table S1 of the Supporting Information.

In the Fourier transform of the EXAFS spectrum of the Pts−PPO400 hybrid matrix, the first peak appears less intense and broader than that measured on the three crystalline references. This feature suggests a larger disorder in the first coordination shell than that encountered in the references compounds. Due to the finite number of parameters which can be varied during the fitting procedure, 4-fold and 5-fold coordination models were used for simulating the EXAFS spectrum of the Pts-PPO400 hybrid. Both models, gathered in Table S1 of the Supporting Information, give a coordination number higher for chlorine atoms than for light atoms, evidencing an effective ligand exchange suffered by the CisPt molecule. The best fit is obtained with a 4-fold coordination for platinum with 1.2 light atoms at 2.05 Å and 2.8 chlorine atoms at 2.28 Å. This result is consistent with the formation of a $(PtCl_3R)^-$ anion, where R can be assigned to NH_3, H_2O, or EtOH. Unfortunately, due to the similar backscattering amplitudes for nitrogen and oxygen atoms in EXAFS spectroscopy, we cannot identify the chemical nature of this R ligand. Nevertheless, the small quantity of water used in the sol−gel reactions, which is essentially consumed into the hydrolysis of $Si(EtO)_3$ moieties, allows us to exclude the hypothesis of the formation of $(PtCl_3H_2O)^-$.[39] Concluding information about the nature of Pts dissolved inside the hybrid was gained from Raman spectroscopy.

Figure 2 compares the crystalline CisPt and K-$(PtCl_3NH_3)\cdot H_2O$ Raman spectra with the unloaded and Pts−PPO400 hybrid ones in the Raman shift range (100−600 cm^{-1}) characteristic of vibrational properties of metal−ligand. The incorporation of Pts in the PPO400 hybrid matrix is confirmed by the presence of well resolved peaks characteristic of

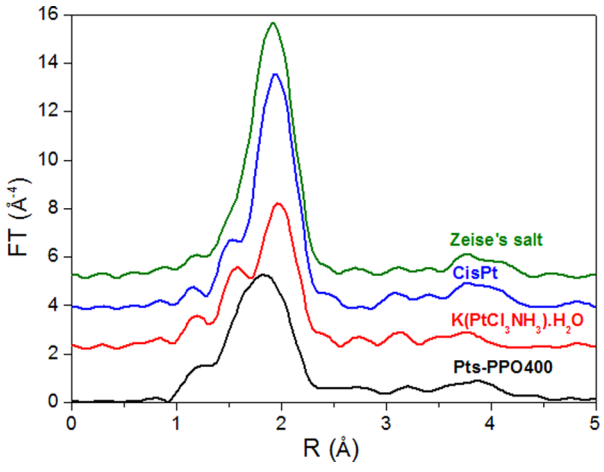

Figure 1. Fourier transforms of the EXAFS spectra of platinum species (Pts) dissolved into the PPO400 hybrid matrix and crystalline references: CisPt, $K(PtCl_3NH_3)\cdot H_2O$, and $K(PtCl_3C_2H_4)\cdot H_2O$ Zeise's salt.

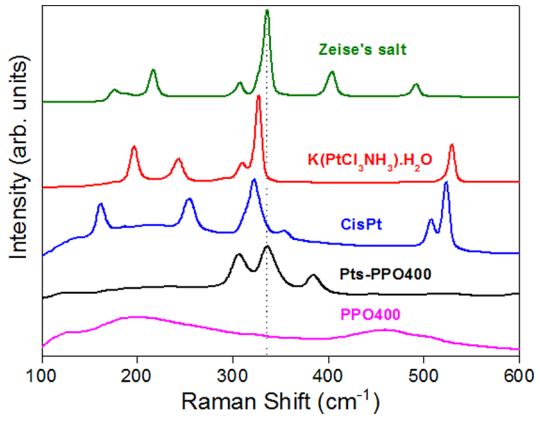

Figure 2. Raman spectra of crystalline references (CisPt, K-$(PtCl_3NH_3)\cdot H_2O$, and $K(PtCl_3C_2H_4)\cdot H_2O$), unloaded PPO400, and Pts−PPO400 hybrids in the region characteristic of the Pt-L vibration bands.

dx.doi.org/10.1021/jp302606b | J. Phys. Chem. B 2012, 116, 7931−7939

platinum−ligand vibrations. The disappearance of the vibration bands related to the Pt−NH_3 moiety of crystalline CisPt at 253 cm^{-1} (δ(N−Pt−N) bending), 506 and 522 cm^{-1} (asymmetric and symmetric ν(Pt−N) stretching) and the splitting of the band at 322 cm^{-1} characteristic of the stretching vibration of the Pt−Cl bond in CisPt into two bands at 305 and 335 cm^{-1} again evidence that the structure of the CisPt moiety has been modified upon loading in the PPO400 matrix.[40] Actually, the splitting of the stretching vibration of the Pt−Cl bond is usually encountered in the Raman spectra of the family of compounds derived from the Zeise's salt[41] and based on the anionic $(PtCl_3R)^-$ species where R = C_2H_4,[41] NH_3, CO,[42] or C_2H_4O.[43]

For comparison purposes, the Raman spectrum of the Zeise's salt is also presented in Figure 2. The bands characteristic of the Pt−Cl stretching vibration in the Zeise's salt are located at 308 and 336 cm^{-1} for the trans chlorine ligand and the cis ones,[41] respectively. These band positions are very close to the values found for the Pts−PPO400 hybrid. This finding is new evidence of the formation of the anionic $(PtCl_3R)^-$ species already proposed from the EXAFS results. The lack of bands related to the ν(Pt−N) stretching mode in the 500−530 cm^{-1} range allows us to conclude that the linkage between the Pt and amine group has been broken. This finding rules out the formation of the anionic $(PtCl_3NH_3)^-$ species. The remaining unidentified band located at 383 cm^{-1} which characterizes the Raman spectrum of the Pts−PPO400 hybrid (Figure 2) can be assigned to the stretching vibration associated to the Pt−O bond. Indeed, several publications report that the υ(Pt−O) vibrations give rise to bands shifted to shorter wavenumbers compared to the υ(Pt−N) vibrations located in the range near 400 cm^{-1}.[44,45]

In summary, the Raman and EXAFS results allow us to propose that the anionic species $(PtCl_3R)^-$ with R = EtOH has been formed and incorporated into the PPO400 hybrid matrix during the one-pot sol−gel processing. In fact, the ESI-mass spectrum recorded for the water solution in which Pts−PPO400 hybrids was immersed for 24 h reveals that the $(PtCl_3EtOH)^-$ molecular ion is released in water from this hybrid matrix. Then, we propose the following scheme for the formation of the $(PtCl_3EtOH)^-$ species:

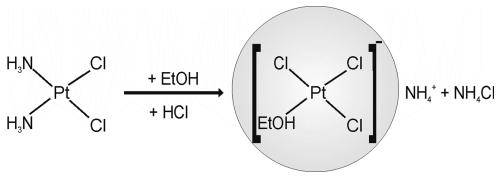

The in-depth structural characterization evidences that, during the one-pot sol−gel synthesis, a ligand exchange reaction inside the liquid-like solvent characterizing the polyether oxygen groups and urea groups of the matrix occurs, leading to the formation of an ionic chloro platinum(II) square planar complex. It is noteworthy that the preparation of ionic square planar complexes from CisPt salt, as $[PtCl_3(NH_3)]^-$ and $[PtCl(A)_2(Am)]^+$ (A = NH_3 or i-$PrNH_2$, Am = pyridine, pyrimidine, purine, or aniline), involves a similar ligand exchange reaction undergoing through the attack of an incoming ligand, which may also occur in association with the solvolysis.[46−48] Thus, in many instances, the direct replacement of ligand, X, by an entering group, Y, must compete with the replacement of X by a solvent molecule. Although sometimes the intermediate may be characterized, frequently the solvent is rapidly substituted by Y.[47,48] Herein, the ether-type oxygen atoms of PE chains and/or the carboxylic groups of the urea which favor the dissolution of the metal salt inside the ureasil−PE hybrid may be considered as a "liquid-like solvent". The ligand exchange reaction inside this liquid-like solvent was clearly demonstrated by the formation $FeCl_4^-$ from the dissolution of Fe(III) nitrate in the presence of excess chlorine ions.[49] Herein, the high propensity of CisPt to exchange both ligands (Cl or NH_3) to form ionic species is responsible for the easier dissolution of the Pt species inside the PPO400 hybrid matrix. It is noteworthy that the ionic square planar complexes, $[PtCl_3(NH_3)]^-$ and $[PtCl(A)_2(Am)]^+$, are today currently investigated as new candidates for platinum-based antitumor drugs.[50,51] Then, the targeted application for the Pts−PPO400 hybrid materials is already relevant for this application, providing that a deeper knowledge of interactions of this species with the hybrid network in the as-prepared sample and during its release in solution is provided.

3.2. Thermal and Nanostructural Features. The DSC profiles of crystalline CisPt, unloaded PPO400, and Pts−PPO400 hybrids are shown in Figure 3a. The lack of the exothermic degradation peak of CisPt at 320 °C confirms that no crystalline CisPt phase is embedded in the hybrid matrix. The shift of the glass transition temperature (T_g) of PPO chains from −38.3 °C for the unloaded hybrid to 28.4 °C for the loaded matrix clearly evidences that the rigidity of the polymeric matrix is strongly increased by the incorporation of Pts. Furthermore, the variation of heat capacity ΔC_p involved in

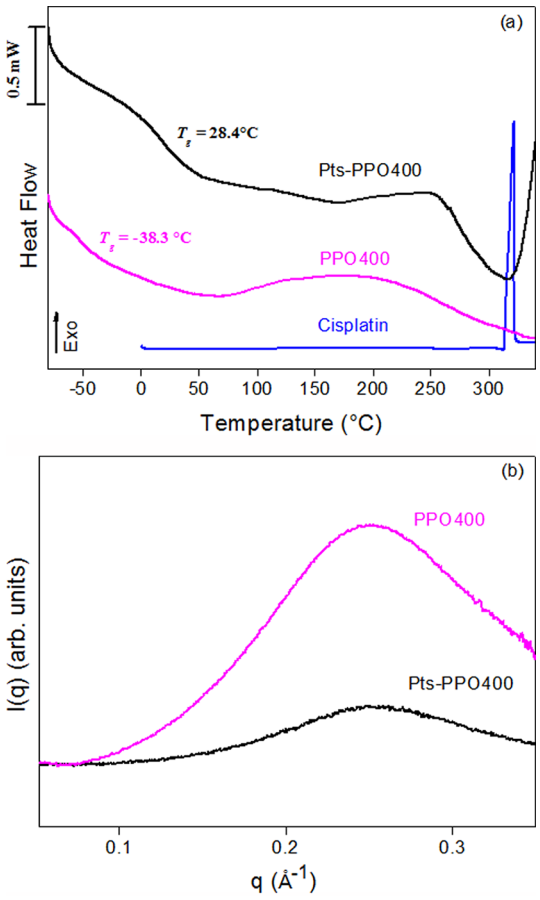

Figure 3. (a) DSC thermograms of crystalline CisPt salt, unloaded PPO400, and Pts−PPO400 hybrids and (b) SAXS curves corresponding to unloaded PPO400 and Pts−PPO400 hybrids.

dx.doi.org/10.1021/jp302606b | J. Phys. Chem. B 2012, 116, 7931−7939

this glass transition phenomenon is about 3 times higher for the Pts−PPO400 hybrid than for the unloaded PPO400 hybrid. These phenomena have already been observed for similar hybrid matrixes loaded with sodium salts[21] and for amorphous PE matrixes complexed with alkali salts.[52,53] Nevertheless, it is noteworthy that, for the sodium salt loaded similar hybrid matrixes,[21] the increase of T_g occurred with a lesser extent (typically 35 °C) and for higher doping level ([O]/[Na] ∼ 1.3) than that used herein ([O]/[Pt] ∼ 35), with [O] being the concentration of ether-type oxygen atoms of the PPO chain. In the absence of undissolved platinum aggregates, this phenomenon can be explained by formation of transient inter/intra PPO chain cross-linking induced by interactions with ionic solutes.[21] Nevertheless, the increase of rigidity of the polymeric backbone in the Pts−PPO400 hybrids observed at so lower doping level compared to sodium doping PPO hybrids[21] suggests that an alternative phenomenon to the metal cation solvation by the ether-type oxygen atoms of the PPO chain could be responsible for this behavior.

The SAXS patterns of the unloaded and Pts−PPO400 hybrids are compared in Figure 3b. Both patterns show a broad peak with a maximum at ∼0.25 $Å^{-1}$ which is usually interpreted as an interference effect in the X-ray scattering amplitude produced by the existence of spatially correlated siloxane-rich domains embedded in the polymeric-rich phase.[21] The strong intensity decrease for this peak observed for the Pts−PPO400 hybrid reveals a decrease of the electronic density contrast between siloxane nodes and polymeric matrix as a consequence of the filling of open space between the polymeric chains by Pts. This finding is complementary evidence of solvation of cations or electropositive species by the ether-type oxygen atoms of the PPO chains.

3.3. PPO400-Platinum Species Interactions. Valuable information about the solvation of $(PtCl_3EtOH)^-$ and its NH_4^+ counterion with different functional groups forming the PPO400 hybrid network may be gained from the analysis of the spectral signatures of polyether backbone and of urea linkage. Figure 4a and b display the Raman spectra recorded for the hybrid samples in the 600−1800 and 2700−3100 cm^{-1} Raman shift ranges, respectively. In the region characteristic of the organic moiety, several additional bands located at 672 (very strong), 704 (strong), 934 (shoulder), 952 (medium), 1028 (strong), 1057 (shoulder), 1312 (weak), 1416 (strong), 2917 (very strong), and 3001 cm^{-1} (strong) are superimposed to the envelope of the characteristic vibrations of the matrix as $NH_4(PtCl_3EtOH)$ is incorporated into the hybrid. We can divide the vibration bands in PPO400 hybrids into three groups, with two of them which have been already reported as strongly influenced by the insertion of dopants.[21,54]

The first group of bands, located in the 800−970 cm^{-1} range, is related to the CH_2 rocking and to the C−O and C−C stretching modes and is very sensitive to the conformation change of the polymeric backbone.[21,54] Its analysis provides information about the interactions between cationic species and ether-type oxygen atoms. For unloaded hybrid, this Raman shift region essentially presents a broad envelop with maxima at 800, 861, 904, and 928 cm^{-1}. After incorporation of the Pts, the band at 861 cm^{-1} is shifted to 869 cm^{-1}, the one at 928 cm^{-1} slightly increases in intensity and shifts to 934 cm^{-1}, and a new intense band at 952 cm^{-1} appears. Those changes were reported in the infrared study of $NaCF_3SO_3$-doped monourethanesil xerogels[55] and interpreted as the fingerprint of the interactions between the Na^+ cations and the ether-type oxygen

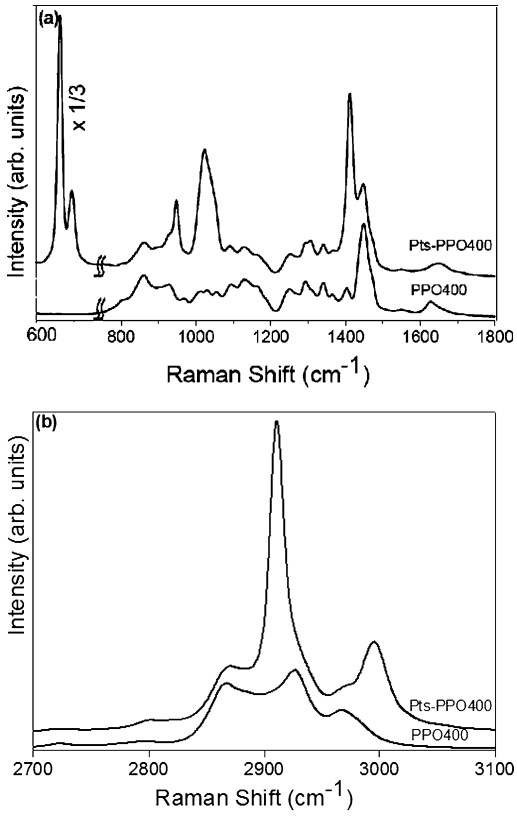

Figure 4. Raman spectra of unloaded PPO400 and Pts−PPO400 hybrids in the region characteristic of the main vibration bands of the hybrid matrix: (a) 600−1800 cm^{-1} and (b) 2700−3100 cm^{-1}.

atoms of the polymeric chains. In the present case, we propose that the intensity increase of bands at 934 and 952 cm^{-1} is the result of interactions between the NH_4^+ cations and the ether-type oxygen of the polymeric backbone. Additionally, upon Pts loading, the Raman spectrum is characterized by the appearance of a strong band at 1028 cm^{-1} with a marked shoulder at 1057 cm^{-1}. Those bands are attributed to the C−O stretching modes. Strong modifications occurring in these bands upon loading are consistent with the interaction of NH_4^+ cations with ether-type oxygen atoms, as schematized in Figure 5a.

The second region located in the 1600−1750 cm^{-1} Raman shift range is related to the so-called amide I vibrations of the urea groups which connect the siloxane nodes to the PPO chain. We observe a shift of the band, from 1630 to 1656 cm^{-1}, when Pts is added to the PPO400 hybrid. This change of the amide I vibration band position toward higher frequency upon the increase of dopant is commonly interpreted as a decrease of the strength of the hydrogen bond network involving the amide groups.[21]

In summary, the changes observed in both regions are indicative of (i) a perturbation of hydrogen bonds mainly ensured by the amide groups of the urea connectors[21,56] and (ii) the formation of interactions between the NH_4^+ cations and the ether-type oxygen atoms of the PPO chain. These findings evidence that the urea and ether-type oxygen coordination sites are both affected by the incorporation of the $NH_4(PtCl_3EtOH)$ into PPO400 hybrids.

In addition, it is important to note that the bands located at 672, 704, 1416, 2917, and 3001 cm^{-1} appear very intense compared to the spectrum of the unloaded hybrid. Thus, these

dx.doi.org/10.1021/jp302606b | J. Phys. Chem. B 2012, 116, 7931−7939

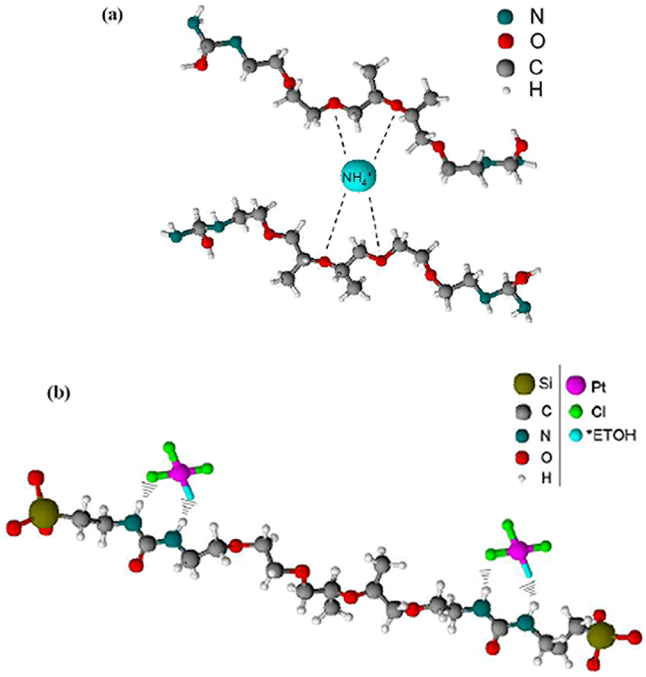

Figure 5. (a) Scheme for the coordination of the NH_4^+ countercation and the ether type oxygen atoms of PPO chains and (b) scheme for the coordination of anionic species $PtCl_3EtOH^-$ and the amine of the urea linkage.

bands are also characteristic fingerprints of the interaction of the Pts with the PPO400 hybrid matrix, as discussed in the following.

A close inspection of the spectrum recorded for the unloaded hybrid in the region 600−800 cm^{-1} reveals very weak resolved bands shifted at higher frequency by 10 cm^{-1} with respect to the strongly intense bands at 672 and 704 cm^{-1}. These bands are usually attributed to wagging NH_2, $\tau(NH_2)$, and $\pi(NH)$ modes characteristic of amide groups.[56,57] Then, a plausible interpretation for the increase of intensity of bands at 672 and 704 cm^{-1} is the occurrence of strong attractive interactions between the anionic species $(PtCl_3EtOH)^-$ and the amine of the urea group involving strong perturbations of the amide V vibrations. Such attraction between anion and urea group, schematized in Figure 5b, is in full agreement with the theoretical investigation made by Saito et al.,[58] which correlates the remarkable effect of $LiPF_6$ salt to the hydrogen bonding interactions involving PF_6^- anions and the hydrogen atoms of the −NH group of urea.

The spectral modifications observed in the 1400−1500 and 2800−3100 cm^{-1} ranges are interrelated; it is appropriate to discuss both Raman shift regions together. In the C−H stretching mode region, the spectrum of the unloaded hybrid presents a broad asymmetric band near 2870 cm^{-1}, a narrower intense band at 2925 cm^{-1}, and a low intensity band at 2975 cm^{-1} attributed to the CH_2 and CH_3 symmetric and asymmetric $\upsilon(CH)$ stretching modes. Upon Pts loading into the hybrid matrix, two strongly intense bands at 2917 and 3001 cm^{-1} appear. The occurrence of intense bands in the C−H stretching region is commonly interpreted as resulting from the strong Fermi resonance interaction between the fundamental symmetric stretching frequency, $\upsilon(CH)$, and the binary combinations of the overtones of appropriate (CH_2) bending modes, $\delta(CH_2)$.[59−61] The spectrum of the Pts−PPO400 presents as well a remarkable enhancement of the intensity of the bending vibrational mode at 1416 cm^{-1} compared to the unloaded matrix. Then, we propose that the bands at 2917 and 3001 cm^{-1} are related to the Fermi resonance interaction between the overtone of this bending CH_2 mode and the $\upsilon(CH)$ stretching vibration of the same symmetry. Actually, the bending region of CH_2 groups for aliphatic chains is well documented in experimental and theoretical studies.[62−64] These works evidence the hypersensibility of the 1416 cm^{-1} band to both the intermolecular interactions between adjacent chains which is crystal structure dependent and the intramolecular interaction involving dispersion of the bending modes parallel to the chain axis.[59] Actually, the reported experimental and calculated Raman spectrum in both CH_2 stretching and bending regions of an isotopically isolated polymethylene n-$C_{36}H_{74}$ chain in n-$C_{36}D_{74}$ (Figures 5 and 6 of ref 59), in which the effect of intermolecular interactions have been minimized, presents strong similarities with the results presented herein. Accordingly, we conclude that the intensity increase of the 1416 cm^{-1} band results from the existence of supramolecular interactions between the guest molecules (NH_4^+ and Pts) and some of the polymeric chains, which hinder direct interactions between PPO chains leading to an "isolate-like state". The coexistence of those chains in an isolate-like state with another family of intermolecular interacting chains gives rise to a "staining" effect similar to the isotope labeling used in ref 59.

Finally, it is important to note that the proposed interaction between urea group and the anionic species is compatible with the change of hydrogen bond network evidenced in the amide I region after Pts incorporation. Furthermore, the intensification of the bending mode at 1416 cm^{-1} associated with the PPO supramolecular effect caused by NH_4^+ solvation by ether-type oxygen atoms, together with the occurrence of Fermi resonance interactions in the stretching CH region, is consistent with the strong increase of the polymeric chain rigidity evidenced by DSC (Figure 3a) and with the homogeneous dispersion of Pts in the polymeric backbone deduced from SAXS results (Figure 3b).

3.4. Effect of Decomplexation of Pt-Species upon Release. In order to describe better the $NH_4(PtCl_3EtOH)$−matrix interaction assumed by both anion−urea and cation−ether type oxygen atoms attractions schematized in Figure 5, we monitor by Raman spectroscopy the kinetics of decomplexation of the immobilized Pts by releasing it in deionized water. Figure 6a and b display the time evolution of the $\upsilon(Pt-Cl)$ and $\upsilon(Pt-O)$ bands and their change in position upon immersion in water of the Pts−PPO400 hybrid, respectively. The three bands continuously decrease in intensity, disappearing after 2 h as a consequence of the release of the anionic species $(PtCl_3EtOH)^-$ in solution, as evidenced by previous UV−vis titrations.[33] It is important to emphasize that the band at 305 cm^{-1} associated to the Pt−Cl(trans) stretching remains invariant in position, whereas those at 335 and 383 cm^{-1} shift at higher frequencies upon release by 5 and 3 cm^{-1}, respectively. These results clearly evidence that the ethanol molecule and the cis-chlorine ligands of the $PtCl_3EtOH^-$ species are both involved in the main interaction with the urea group, as displayed in Figure 5b.

Figure S2 of the Supporting Information displays the time evolution of the bands in the 600−800, 800−1800, and 2750−3100 cm^{-1} ranges upon immersion in water of the Pts−PPO400 hybrid, respectively. Figure 7 shows the frequency

dx.doi.org/10.1021/jp302606b | J. Phys. Chem. B 2012, 116, 7931−7939

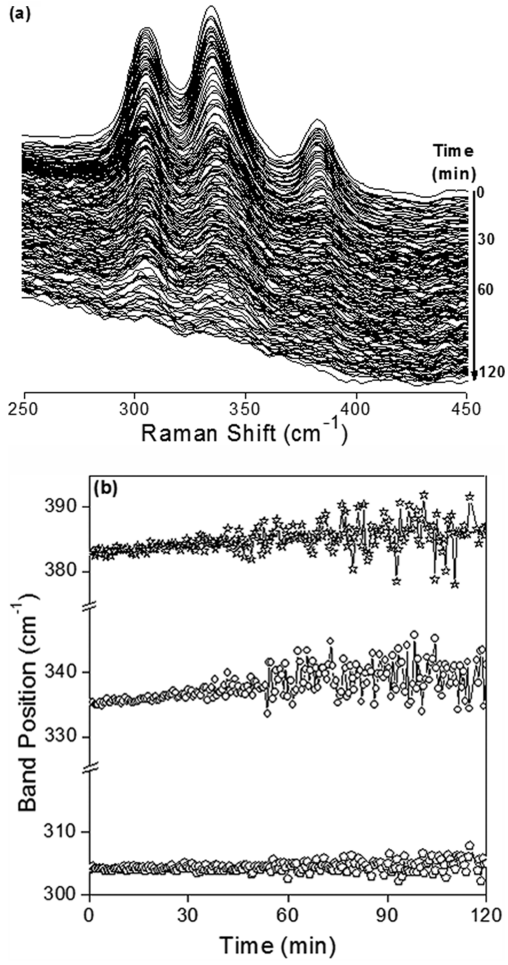

Figure 6. Time evolution of the Raman data during the release of Pts–PPO400 hybrid upon immersion in water: (a) Spectra in the region of υ(Pt–Cl) and υ(Pt–O) bands and (b) changes in υ(Pt–Cl) and υ(Pt–O) band position.

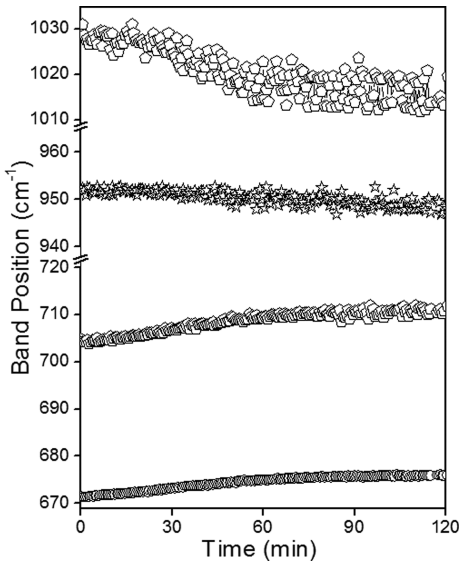

Figure 7. Time evolution of the position of the Raman bands during release of Pts–PPO400 hybrid upon immersion in water.

change of the maximum of the bands presenting a decrease in intensity upon Pts release. As observed for the characteristic vibration bands of the $PtCl_3EtOH^-$ moiety, the bands at 672 and 704 are also shifted by 5 cm^{-1}. This feature is another manifestation of hardening of vibrational modes characteristic of amide groups upon Pts deloading. These results evidence again for the preferential complexation of $PtCl_3EtOH^-$ by the urea linkage present at the organic–inorganic interface of the hybrid matrix.[56]

On opposition, upon release, the bands originally centered at 952 and 1028 cm^{-1} associated to the interaction of NH_4^+ with the ether-type oxygen atoms are shifted by −4 and −10 cm^{-1}, respectively. To interpret this behavior, it is also necessary to consider the change of the position of the amide I vibration upon release in water. This band initially located at 1656 cm^{-1} is shifted to 1637 cm^{-1}, which is practically the position found in the unloaded PPO400 matrix. These red shifts evidence that the hydrogen bonding structure involving both hydrogen atoms of the NH amide group of the urea linkage and the ether-type oxygen atoms of the polymeric matrix are recovered upon Pts decomplexation. Then, these results demonstrate that the incorporation of $NH_4(PtCl_3EtOH)$ into the PPO400 matrix affects in a reversible way the hydrogen bonding structure characteristic of this kind of hybrid materials.

4. CONCLUSIONS

The one-pot sol–gel process coupled to the ligand exchange reaction of the square planar Pt(II) complex was used to synthesize ureasil cross-linked PPO hybrid materials incorporating a Zeise's type salt NH_4 ($PtCl_3$ EtOH), derivative from CisPt. The efficiency of the ligand exchange reaction and of the random dissolution of Pt salt into ureasil–PPO hybrid was clearly evidenced by the combination of several experimental techniques.

The in-depth Raman analyses revealed that the dissolution of the NH_4 ($PtCl_3$ EtOH) salt into the ureasil–PPO matrix is intrinsically related to the multifunctional feature of the hybrid framework, in particular for hosting simultaneously anionic and cationic species. The analysis of the specific vibrational modes of the PPO backbone evidenced that the coordination of NH_4^+ cations occurs by preferential interactions with ether-type oxygen atoms of the polyether chains. The preferential complexation of the $PtCl_3EtOH^-$ anions by the urea linkage present at the organic–inorganic interface of the hybrid matrix was evidenced by the changes of the characteristics of the amide I and amide V vibration bands after Pts incorporation into PPO400 hybrid.

The time evolution of the position of the υ(Pt–Cl) and υ(Pt–O) bands during decomplexation clearly evidenced that the ethanol molecule and the cis-chlorine ligands of the $PtCl_3EtOH^-$ species are both involved in the main interaction with the urea group. The formation of both cation–ether type oxygen atoms and anion–urea group supramolecular interactions gives rise to a partial destruction of the original hydrogen-bonded network between PPO/urea resulting in a strong decrease of the PPO chain mobility.

The reversible recovery of the structural features of PPO400 hybrid after NH_4 ($PtCl_3$ EtOH) decomplexation induced by release in water combined with the reversibility of the ligand exchange reaction can inspire the design of the simple one-pot sol–gel route and also of new advanced materials for controlled delivery devices of active Pt species with emerging applications for the cancer therapy and for homogeneous catalysis.

dx.doi.org/10.1021/jp302606b | J. Phys. Chem. B 2012, 116, 7931–7939

■ ASSOCIATED CONTENT

Supporting Information

Figures showing the evolution of the Raman spectra during the wet gel−xerogel conversion of Pts−PPO400 hybrid and during the release of Pts−PPO400 hybrid upon immersion in water. Table gathering the structural parameters determined by EXAFS for the Pts−PPO400 hybrid. This material is available free of charge via the Internet at http://pubs.acs.org.

■ AUTHOR INFORMATION

Corresponding Author

*E-mail: efmolina@iq.unesp.br (E.F.M.); briois@synchrotron-soleil.fr (V.B.). Phone: +33 1 69 35 96 44. Fax: +33 1 69 35 94 56.

Notes

The authors declare no competing financial interest.

■ ACKNOWLEDGMENTS

We acknowledge the financial support received from the Brazilian agencies, namely, the CAPES, CNPq, and FAPESP and the French COFECUB agency (Project Number Ph 564/07). SOLEIL (France) and LNLS (Brazil) are readily acknowledged for the technical and financial support provided during the EXAFS and SAXS measurements.

■ REFERENCES

(1) Schottner, G. *Chem. Mater.* **2001**, *13*, 3422−3435.
(2) Sanchez, C.; Julian, B.; Belleville, P.; Popall, M. *J. Mater. Chem.* **2005**, *15*, 3559−3592.
(3) Sanchez, C.; Belleville, P.; Popall, M.; Nicole, L. *Chem. Soc. Rev.* **2011**, *40*, 696−753.
(4) Rossi, D.; Carpi, F.; Scilingo, E. P. *Adv. Colloid Interface Sci.* **2005**, *116*, 165−178.
(5) Walcarius, A.; Collinson, M. M. *Annu. Rev. Anal. Chem.* **2009**, *2*, 121−143.
(6) Geng, L; Zhao, Y.; Huang, X.; Wang, S.; Zhang, S.; Wu, S. *Sens. Actuators, B* **2007**, *120*, 568−572.
(7) Descalzo, A; B.; Martinez-Mánez, R.; Sancenón, F.; Hoffmann, K.; Rurack, K. *Angew. Chem., Int. Ed.* **2006**, *45*, 5924−5948.
(8) Pardo, R.; Zayat, M.; Levy, D. *Chem. Soc. Rev.* **2011**, *40*, 672−687.
(9) Kawasaki, N.; Wang, H.; Nakanishi, R.; Hamanaka, S.; Kitaura, R.; Shinohara, H.; Yokoyama, T.; Yoshikawa, H.; Awaga, K. *Angew. Chem., Int. Ed.* **2011**, *50*, 1−5.
(10) Yuan, J.; Xu, Y.; Müller, A. H. E. *Chem. Soc. Rev.* **2011**, *40*, 640−655.
(11) Ruiz-Hitzky, E.; Aranda, P.; Dardera, M.; Rytwo, G. *J. Mater. Chem.* **2010**, *20*, 9306−9321.
(12) Choi, S.; Choi, G; E.; Oh, J.; Oh, Y; Park, M; Choy, J. *J. Mater. Chem.* **2010**, *20*, 9463−9469.
(13) Chang, Y; Allcock, H; R. *Chem. Mater.* **2005**, *17*, 4449−4454.
(14) Zhu, Y; Shi, J.; Shen, W.; Dong, X.; Feng, J.; Ruan, M.; Li, Y. *Angew. Chem., Int. Ed.* **2005**, *44*, 5083−5087.
(15) Nakanishi, K.; Tanaka, N. *Acc. Chem. Res.* **2007**, *40*, 863−873.
(16) Carlos, L. D.; Ferreira, R. A. S.; Bermudez, V. Z.; Ribeiro, S. J. L. *Adv. Mater.* **2009**, *21*, 509−534.
(17) Innocenzi, P.; Lebeau, B. *J. Mater. Chem.* **2005**, *15*, 3821−3831.
(18) Serbin, J.; Egbert, A.; Ostendorf, A.; Chichkov, B. N.; Houbertz, R.; Domann, G.; Schulz, J.; Cronauer, C.; Fröhlich, L.; Popall, M. *Opt. Lett.* **2003**, *28*, 301−303.
(19) Dahmouche, K.; De Souza, P. H.; Bonagamba, T. J.; Paneppucci, H.; Judeinstein, P.; Pulcinelli, S. H; Santilli, C. V. *J. Sol-Gel Sci. Technol.* **1998**, *13*, 909−913.
(20) Mello, N. C.; Bonagamba, T. J.; Panepucci, H.; Dahmouche, K.; Judeinstein, P.; Aegerter, M. A. *Macromolecules* **2000**, 33, 1280−1288.
(21) Chaker, J. A.; Santilli, C. V.; Pulcinelli, S. H.; Dahmouche, K.; Briois, V.; Judeinstein, P. *J. Mater. Chem.* **2007**, *17*, 744−757.
(22) Carlos, L. D.; Bermudez, V. D.; Ferreira, R. A. S. *J. Non-Cryst. Solids* **1999**, *247*, 203−208.
(23) Brankova, T.; Bekiari, V.; Lianos, P. *Chem. Mater.* **2003**, *15*, 1855−1859.
(24) Fu, L. S.; Ferreira, R. A. S.; Silva, N. J. O.; Fernandes, J. A.; Ribeiro-Claro, P.; Goncalves, I. S.; Bermudez, V. D.; Carlos, L. D. *J. Mater. Chem.* **2005**, *15*, 3117−3125.
(25) Makris, T.; Dracopoulos, V.; Stergiopoulos, T.; Lianos, P. *Electrochim. Acta* **2011**, *56*, 2004−2008.
(26) Chiavacci, L. A.; Dahmouche, K.; Silva, N. J. O.; Carlos, L. D.; Amaral, V. S.; Bermudez, V. D.; Pulcinelli, S. H.; Santilli, C. V.; Briois, V.; Craievich, A. F. *J. Non-Cryst. Solids* **2004**, *345*, 585−590.
(27) Silva, N. J. O.; Amaral, V. S.; Bermudez, V. D.; Nunes, S. C.; Ostrovskii, D.; Rocha, J.; Carlos, L. D. *J. Mater. Chem.* **2005**, *15*, 484−490.
(28) Riccardi, C. S.; Dahmouche, K.; Santilli, C. V.; Costa, P. I.; Yamanaka, H. *Talanta* **2006**, *70*, 637−643.
(29) Bekiari, V.; Lianos, P. *Chem. Mater.* **2006**, *18*, 4142−4146.
(30) Santilli, C. V.; Chiavacci, L. A.; Lopes, L.; Pulcinelli, S. H.; Oliveira, A. G. *Chem. Mater.* **2009**, *21*, 463−467.
(31) Lopes, L.; Molina, E. F.; Chiavacci, L. A.; Santilli, C. V.; Briois, V.; Pulcinelli, S. H. *RSC Adv.* **2012**, *2*, 5629−5636.
(32) Molina, E. F.; Pulcinelli, S. H.; Santilli, C. V.; Blanchandin, S.; Briois, V. *J. Phys. Chem. B* **2010**, *114*, 3461−3466.
(33) Molina, E. F.; Santilli, C. V.; Pulcinelli, S. H.; Blanchandin, S.; Baudelet, F.; Briois, V. *Phase Transitions* **2011**, *84*, 687−699.
(34) Briois, V.; Fonda, E.; Belin, S.; Barthe, L.; La Fontaine, C.; Langlois, F.; Ribbens, M.; Villain, F. *UVX 2010 EDP Sciences* **2011**, 41−47.
(35) Milburn, G. H. W.; Truter, M. R. *J. Chem. Soc. A* **1966**, *19*, 1609−1616.
(36) Oksanen, A.; Leskela, M. *Acta Chem. Scand.* **1994**, *48*, 485−488.
(37) Love, R. A.; Koetzle, T. F.; Williams, G. J. B.; Andrews, L. C.; Bau, R. *Inorg. Chem.* **1975**, *14*, 2653−2657.
(38) Ravel, B.; Newville, M. *J. Synchrotron Radiat.* **2005**, *12*, 537−541.
(39) Deeth, R. J.; Elding, L. I. *Inorg. Chem.* **1996**, *35*, 5019−5026.
(40) Michalska, D.; Wysokinski, F. *Chem. Phys. Lett.* **2005**, *403*, 211−216.
(41) Hiraishi, J. *Spectrochim. Acta, Part A* **1969**, *25*, 749−760.
(42) Denning, R. G.; Ware, M. J. *Spectrochim. Acta, Part A* **1968**, *24*, 1785−1793.
(43) Crayston, J. A.; Davidson, G. *Spectrochim. Acta, Part A* **1987**, *43*, 559−564.
(44) Iakovidis, A.; Hadjiliadis, N.; Butler, I. S. *Spectrochim. Acta, Part A* **1991**, *47*, 1567−1574.
(45) Condrate, R. A.; Nakamoto, K. *J. Chem. Phys.* **1965**, *42*, 2590−2598.
(46) Helm, L.; Merbach, A. E. *Chem. Rev.* **2005**, *105*, 1923−195.
(47) Dedieu, A. *Chem. Rev.* **2000**, *100*, 543−600.
(48) Mureinik, R. J. *Coord. Chem. Rev.* **1978**, *25*, l−30.
(49) Chiavacci, L. A.; Dahmouche, K.; Briois, V.; Santilli, C. V.; Bermudez, V. D.; Carlos, L. A.; Jolivet, J. P.; Pulcinelli, S. H.; Craievich, A; F. *J. Appl. Crystallogr.* **2003**, *36*, 405−409.
(50) Macquet, J. P.; Butuor, J. L. *J. Natl. Cancer Inst.* **1983**, *70*, 899−905.
(51) Hollis, L. S.; Amundsen, A. R.; Stern, E. W. *J. Med. Chem.* **1989**, *32*, 128−136.
(52) Vachon, C.; Vasco, M.; Perrier, M.; Prud'homme, J. *Macromolecules* **1993**, *26*, 4023−4031.
(53) Vachon, C.; Labreche, C.; Vallee, A.; Besner, S.; Dumont, M.; Prud'homme, J. *Macromolecules* **1995**, *28*, 5585−5594.
(54) Yoon, S.; Ichikawa, K.; MacKnight, W. J.; Hsu, S. L. *Macromolecules* **1995**, *28*, 4278−4283.
(55) Gonçalves, M. C.; Bermudez, V. D.; Ostrovskii, D.; Carlos, L. D. *Electrochim. Acta* **2003**, *48*, 1977−1989.
(56) Bermudez, V. D.; Carlos, L. D.; Alcacer, L. *Chem. Mater.* **1999**, *11*, 569−580.

(57) Wolf, I.; Desseyn, H. O.; Perlepes, S. P. *Spectrochim. Acta, Part A* **1994**, *50*, 1141−1152.
(58) Saito, Y; Kataoka, H.; Murata, S.; Uetani, Y; Kii, K.; Minamizaki, Y. *J. Phys. Chem. B* **2003**, *107*, 8805−8811.
(59) Snyder, R. G.; Hsu, S. L.; Krimm, S. *Spectrochim. Acta, Part A* **1978**, *34*, 395−406.
(60) Yu, Y; Lin, K.; Zhou, X.; Wang, H.; Liu, S.; Ma, X. *J. Phys. Chem. C* **2007**, *111*, 8971−8978.
(61) Hill, I. R.; Levin, I. W. *J. Chem. Phys.* **1979**, *70*, 842−851.
(62) Abbate, S.; Zerbi, G.; Wunder, S. L. *J. Phys. Chem.* **1982**, *86*, 3140−3149.
(63) Lagaron, J. M. *J. Mater. Sci.* **2002**, *37*, 4101−4107.
(64) Lagaron, J. M.; Powell, A. K.; Davidson, N. S. *Macromolecules* **2000**, *33*, 1030−1035.